Available online at www.sciencedirect.com
SCIENCE DIRECT
Earth and Planetary Science Letters 237 (2005) 680–694
EPSL
www.elsevier.com/locate/epsl

Seismic properties of the inner core boundary from PKiKP/P amplitude ratios

Keith D. Koper *, Marina Dombrovskaya

Department of Earth and Atmospheric Sciences, Saint Louis University, St. Louis, MO 63103, USA

Received 7 December 2004; received in revised form 22 June 2005; accepted 6 July 2005
Available online 10 August 2005
Editor: R.D. van der Hilst

Abstract

A recent study of PKiKP/PcP amplitude ratios found surprisingly low values for the change in density ($\Delta\rho_{ICB}=0.3$ g/cm^3) and shear velocity ($\Delta S_{ICB}=2.0$ km/s) across the inner core boundary (ICB). However, because the data set was limited to small source–receiver distances (<50°) there was a significant trade-off between the two parameters, with higher values in one parameter nearly compensated by higher values in the other. In this study we augment the existing PKiKP/PcP data set with new observations of PKiKP/P amplitude ratios at larger distances (50–90°), and jointly model the two data sets. Considering assumptions in the modeling and observational errors we estimate $\Delta\rho_{ICB}=0.52\pm0.24$ g/cm^3 and $\Delta S_{ICB}=2.82\pm0.32$ km/s. These values can be reconciled with the slightly higher values obtained from normal mode analysis if the outermost inner core is either structurally or chemically distinct from the bulk of the inner core. The new PKiKP/P amplitude ratios show dramatic variation but are geographically coherent; this suggests that significant lateral heterogeneity is present at, or just below, the ICB.

Keywords: inner core boundary; PKiKP; Seismic array

1. Introduction

Recently there has been renewed interest among seismologists in constraining the density jump at the inner core boundary ($\Delta\rho_{ICB}$). This quantity has important implications for models of Earth's magnetic field because it is thought that the geodynamo is primarily driven by the compositional buoyancy of a non-metallic light element that is preferentially segregated into the outer core as the inner core freezes. A large $\Delta\rho_{ICB}$ implies that little light element is incorporated into the solid inner core, and so the light-element induced compositional buoyancy at the base of the outer core acts as a significant driving force for core convection. A small $\Delta\rho_{ICB}$ at the ICB implies the opposite, and if the value is too small it may become problematic to generate core convection at all [1].

The value of $\Delta\rho_{ICB}$ also has implications for observing the Slichter mode triplet that represents the translational motion of the solid inner core with

* Corresponding author. Tel.: +1 314 977 3197; fax: +1 314 977 3117.
E-mail address: koper@eas.slu.edu (K.D. Koper).

0012-821X/$ - see front matter © 2005 Elsevier B.V. All rights reserved.
doi:10.1016/j.epsl.2005.07.013

respect to the outer core. Although it has been pursued for decades, this triplet of modes has never been conclusively identified in seismic or geodetic data [2]. Researchers have generally searched for signals with periods greater than 5 h, which is what is predicted for a standard Earth model with $\Delta\rho_{ICB}=0.60$ g/cm^3 [3]. However, if $\Delta\rho_{ICB}=0.37$ g/cm^3 for example, the theoretical Slichter periods would increase by 25–30% [4]. Similarly, a larger density jump at the ICB would lead to much shorter Slichter periods.

Seismic inference of $\Delta\rho_{ICB}$ is based on two types of data. The first is the eigenfrequencies of Earth's normal modes that are excited by large earthquakes. The second is the amplitudes of body waves (PKiKP) reflected at the ICB. Historically, the mode data supported values of 0.55–0.60 g/cm^3 [5,6], while the body wave data supported values larger than 1.0 g/cm^3 (see [7] for an overview). The mode values were considered more robust and were accepted by the geophysical community because of a possible selection bias in observing precritical PKiKP waves [8], and the general instability of high-frequency body wave amplitudes. Recently, seismologists have used both approaches to place new constraints on $\Delta\rho_{ICB}$: detailed analysis of an expanded mode data set led to a value of 0.82 ± 0.18 g/cm^3 [9]; modeling of over 200 PKiKP/PcP amplitude ratios from short-period array stations led to a value of 0.3 g/cm^3 with an upper bound of about 0.45 g/cm^3 [10]; and modeling of 20 high-quality PKiKP/PcP amplitude ratios mainly from individual broadband seismometers led to a value of 0.6–0.9 g/cm^3 [11].

Much of the scatter in the seismic estimates of $\Delta\rho_{ICB}$ may be due to differences in data processing and modeling assumptions, however there are also interesting explanations based solely on Earth structure. It could be that the ICB has significant lateral variations and that the PKiKP waves used by [10] and [11] led to strikingly different values of $\Delta\rho_{ICB}$ because they sampled different portions of the ICB. Although some seismic studies argue for relatively homogeneous models of the inner core (e.g., [12,13]) others present evidence for a surprising amount of lateral heterogeneity in the inner core [14–19]; it could be that the heterogeneity and/or complexity exists all the way up to the ICB itself. It is also possible to reconcile the PKiKP based value of 0.3 g/cm^3 [10] with the mode-based value of 0.82 ± 0.18 g/cm^3 [9] if the inner core has sharp radial heterogeneity. The PKiKP data are only sensitive to about the outermost 5 km of the inner core, while the mode data are sensitive to radial averages on the scale of hundreds of kilometers. Therefore, a thin layer in the outermost inner core, with density intermediate between the outer core and the bulk of the inner core, could satisfy both types of data simultaneously.

In this paper we seek to refine a previous seismic estimate for $\Delta\rho_{ICB}$ using an expanded data set of PKiKP amplitudes. The new data set consists of about 180 estimates of PKiKP/P amplitude ratios at distances of 50–90°. It includes both positive observations and negative, "upper-limit", observations, all of which are corrected for the radiation pattern of the source. We combine these data with an existing set of PKiKP/PcP amplitude ratios at distances of 10–50° [10]. The new data have different sensitivity to the jumps in P-velocity at the ICB (ΔP_{ICB}), S-velocity at the ICB (ΔS_{ICB}), and $\Delta\rho_{ICB}$, and help alleviate the trade-offs that exist when only the PKiKP/PcP data are considered.

2. Sensitivity of PKiKP/P amplitude ratios

Although high-frequency body wave amplitudes are influenced by many factors, PKiKP/P amplitude ratios are one of the few seismic observations that have significant sensitivity to ΔS_{ICB} and $\Delta\rho_{ICB}$. By using amplitude ratios, rather than direct PKiKP amplitudes, several factors are mitigated: the instrument response, the size of the source, and structural heterogeneities near the source and receiver. It is also routine for centroid moment tensors (CMT) of large earthquakes to be inferred, and these CMT solutions can be used to account for the radiation pattern of the source. Unfortunately, there is still a large discrepancy between the PKiKP and P ray paths (Fig. 1), and so lateral variations in lower mantle structure will affect the amplitude ratios, which could in turn lead to biased inferences of ICB structure. Nevertheless, because of the relatively poor constraints on ΔS_{ICB} and $\Delta\rho_{ICB}$ and the importance of these values in understanding the composition and dynamics of the core, a critical examination of the available data is worthwhile. This is especially true because the sensi-

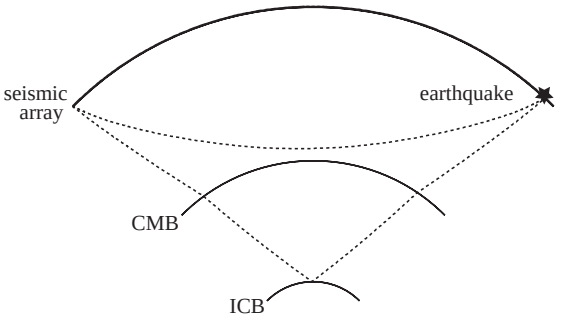

Fig. 1. Ray paths for P and PKiKP at a distance of 85°. PKiKP/P amplitude ratios are one of the few seismological observations that have significant sensitivity to the shear velocity at the top of the inner core.

tivity of PKiKP amplitude to ICB properties is strongly dependent on ray parameter, and PKiKP/P amplitude ratios at larger distances (>50°) provide complementary information to the more robust PKiKP/PcP amplitude ratios observed at smaller distances (<50°).

We present the sensitivity of PKiKP/P amplitude ratios to variations in ICB properties in Fig. 2. The theoretical ratios were calculated using ray theory and account for variations in geometrical spreading and anelastic attenuation via numerical integration of the appropriate expressions through PREM [5]. The vertical component of the amplitudes was used, and no allowance was made for the radiation pattern, thus the curves are appropriate for isotropic sources. Beyond about 90° the ray-theoretical P amplitude drops significantly and the geometrical spreading calculation becomes unstable because the ray parameter changes very slowly just before diffraction begins. The amplitude ratios are most dependent on reasonable variations in ΔS_{ICB} and least dependent on reasonable variations in $\Delta\rho_{ICB}$. However, these two parameters trade-off directly when constrained only by PKiKP/PcP amplitude ratios [10], and so the increased sensitivity to ΔS_{ICB} given by the PKiKP/P ratios leads to a better estimate of $\Delta\rho_{ICB}$ when the two data sets are combined.

3. Data processing

We searched for PKiKP waveforms using data recorded by the short-period, small-aperture arrays of the International Monitoring System (IMS). Coherence based stacking procedures can be used to high frequencies at IMS arrays, and previous studies have shown precritical PKiKP to be observable with such processing. We selected a total of about 180 events that occurred during the open IMS period of 1995–2001, were at distances of 50–90° from an IMS array, had a theoretical PKiKP radiation pattern coefficient of at least 0.75, and were deeper than 50 km. The conditions were chosen to maximize the odds of observing PKiKP, and to allow for the possibility of

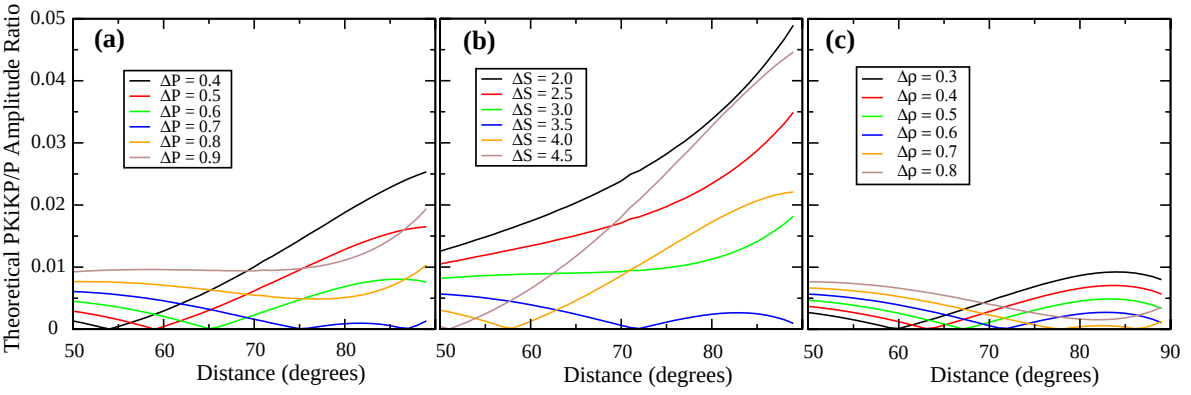

Fig. 2. The sensitivity of theoretical PKiKP/P amplitude ratios to variations in (a) the P velocity (km/s) jump across the ICB, (b) the S velocity (km/s) jump across the ICB, and (c) the density (g/cm^3) jump across the ICB. In all cases the absolute value of the amplitude ratio is presented. At these distances the amplitude ratios are most sensitive to the jump in S velocity across the ICB, and so are complementary to PKiKP/PcP amplitude ratios at smaller distances, which are most sensitive to the density jump across the ICB.

using null observations to estimate upper bounds on PKiKP amplitude. The geographical distribution and other details of the data set are more fully described elsewhere [20].

We examined each event-array combination for the existence of a PKiKP wave using a sliding window, time-domain beamforming process. Observations were initially graded positive if there was a simultaneous spike in beam power, spike in coherence, and drop in ray parameter at the predicted PKiKP arrival time. An example is shown in Fig. 3. These observations were then confirmed as positive with a high-precision estimate of the 2D slowness vector that included bootstrap-derived uncertainties (Fig. 4). A second class of data showed some evidence for a PKiKP arrival but were not clearly positive, and these data were graded inconclusive. The majority of the data showed no evidence for a PKiKP arrival at the expected time and were graded negative.

For each positive observation we measured the PKiKP/P amplitude ratio using a method previously developed to measure PKiKP/PcP amplitude ratios [10]. The method measures peak amplitudes from optimally tuned array beams and generates error bounds based on a bootstrap type resampling process. For the observations graded inconclusive or negative, we generated upper bound estimates on

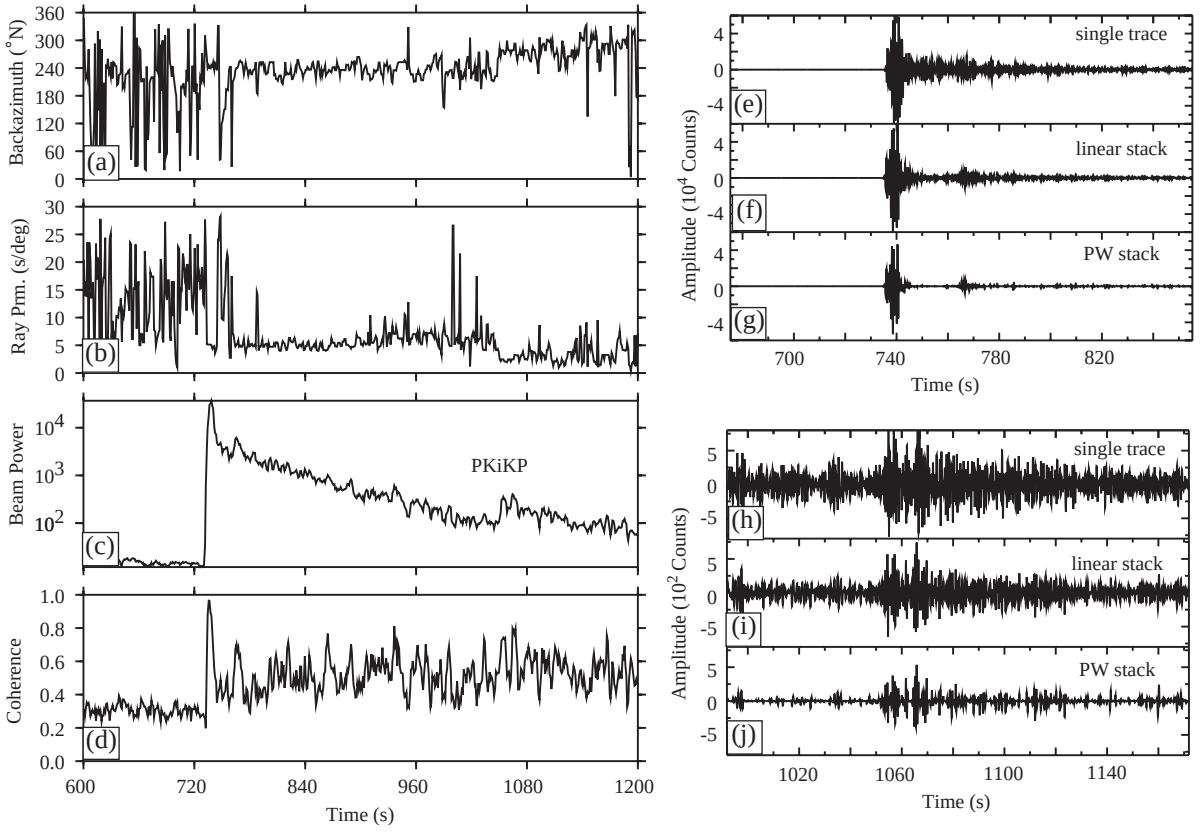

Fig. 3. Example of a positive observation of PKiKP. This 6.4 mb event occurred at a distance of 83.5° from ILAR, on 1998/07/16, with a hypocenter of 11.0 S, 166.2 E, 110 km. The theoretical backazimuth is 226 N, the theoretical arrival times for P and PKiKP are 735 s and 1052 s, and the corresponding theoretical ray parameters are 5.1 s/deg and 1.6 s/deg. Panels (a–d) show the results of a sliding window slowness analysis, in a frequency band centered at 4 Hz, using a window length of 2 s and a window spacing of 1 s. Details of the processing are given elsewhere [20]. The P waveform is shown on (e) a single trace, (f) a linear beam formed at the theoretical P slowness, and (g) a phase weighted beam formed at the theoretical P slowness. Likewise for the PKiKP wave in panels (h–j). An animation of the time evolution of beam power as a function of slowness vector is available as an electronic supplement.

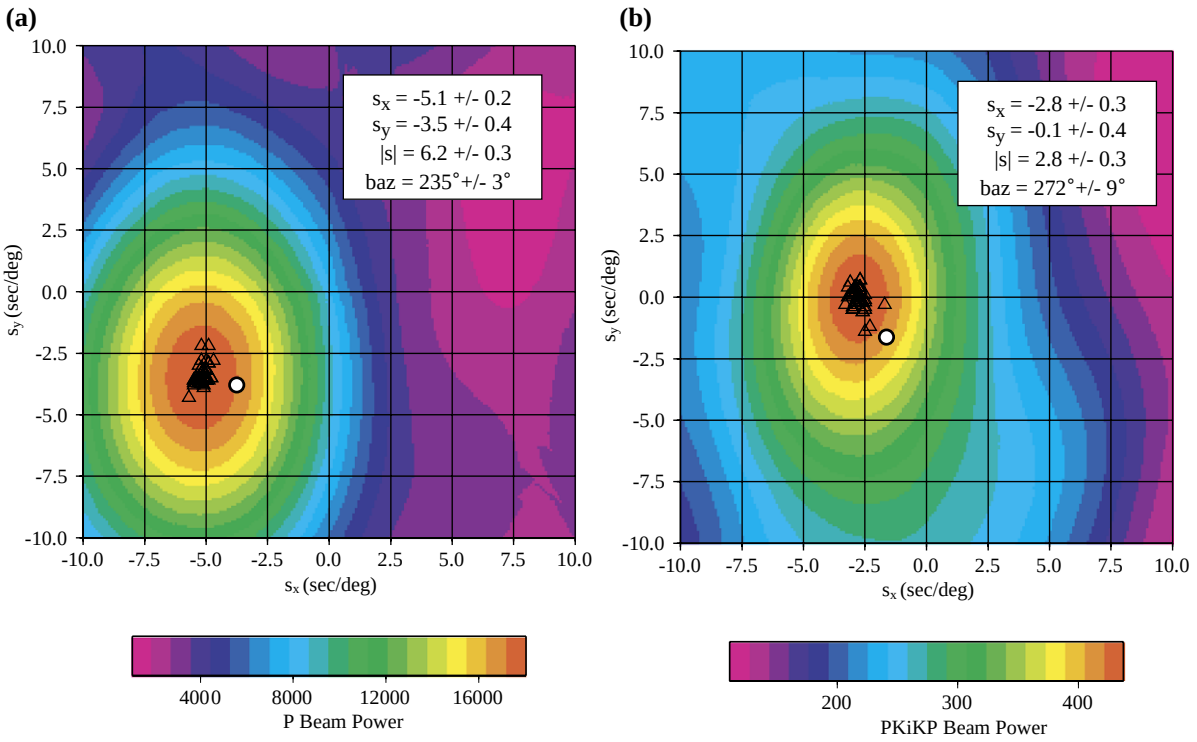

Fig. 4. High precision estimate of the optimal 2D slowness vectors for time windows bracketing the (a) P phase and (b) the PKiKP phase, for the event presented in Fig. 3. The grid search was carried out using increments of 0.1 s/deg for both s_x and s_y and beam power was defined as the root-mean-square amplitude (proportional to ground velocity) in the time window. The white circles represent the theoretical slowness values, and the triangles show the optimal slowness vectors found for 50 bootstrap iterations. Each one of these solutions was determined using a grid search of a pseudo-array formed by randomly resampling (with replacement) the elements of the true array. Slowness anomalies of 1–2 s/deg are common at IMS arrays because of the small apertures.

PKiKP/P amplitude ratios by taking the maximum amplitude in a time window of 3–4 s that bracketed the theoretical PKiKP arrival time, using an array beam formed with the theoretical PKiKP slowness vector.

The PKiKP/P measurements are presented in Fig. 5. Each value has been corrected for source mechanism effects using the appropriate Harvard CMT solution [21]. There is wide scatter in the null and inconclusive data however there are three clusters of positive observations that are geographically coherent. For two of these clusters, near 74° and 85°, the positive data have PKiKP/P amplitude ratios that are 1–2 orders of magnitude larger than the predictions from the standard model (PREM); these data are more consistent with the ICB models derived from PKiKP/PcP amplitude ratios. However, there are many null observations at a variety of distances that fall below the PKiKP/P amplitude levels predicted by the body wave models. Although each null observation cannot be considered a strict upper bound for constraining ICB properties (because of the influence of variations in P amplitude) it appears that an ICB model predicting amplitude ratios intermediate between the three curves shown in Fig. 5 would be the most appropriate global average.

The dramatic variability and scatter in our PKiKP observations is best illustrated by considering the seismograms recorded at the Eielson Array (ILAR) in Alaska. Of the 58 events recorded at ILAR, 10 from the Tonga–Fiji subduction zone are positive for PKiKP and have PKiKP/P amplitude ratios 1–2 orders of magnitude larger than expected, three events from the New Hebrides trench are positive for PKiKP but have normal PKiKP/P amplitude ratios, one event

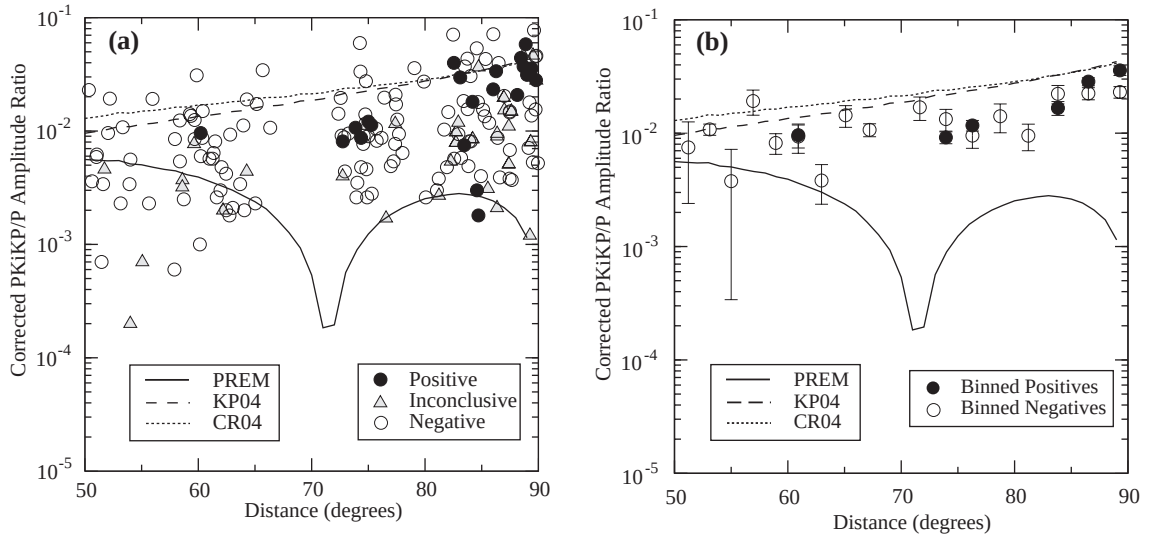

Fig. 5. (a) PKiKP/P amplitude ratios for the 181 source–receiver combinations examined in this study. The black circles indicate definite PKiKP observations, the grey triangles indicate inconclusive observations, and the white circles indicate null observations. In the case of the negative and inconclusive observations an upper bound to the PKiKP amplitudes was measured from a beam formed at the theoretical PKiKP slowness. Error bounds were calculated for each observation using a bootstrap resampling process, but to avoid clutter they are not shown. In all cases the amplitude ratios have been corrected for the source radiation pattern using the Harvard CMT solution. (b) The results of averaging the positive and negative observations in 2 s/rad bins of theoretical PKiKP slowness. The curves show predicted PKiKP/P amplitude ratios for three models that have the same ΔP_{ICB} value: PREM [5], with $\Delta\rho_{ICB}=0.60$ g/cm^3, $\Delta S_{ICB}=3.5$ km/s; KP04 [10], with $\Delta\rho_{ICB}=0.3$ g/cm^3, $\Delta S_{ICB}=2.0$ km/s; and CR04 [11], with $\Delta\rho_{ICB}=0.85$ g/cm^3, $\Delta S_{ICB}=2.5$ km/s.

from the Solomon Islands is positive for PKiKP with a ratio 10 times larger than expected, and the remaining events are either inconclusive or negative for PKiKP. Source information for the events with confirmed PKiKP arrivals at ILAR is listed in Table 1, maps of the source–receiver geometry are presented in

Table 1
Earthquakes with confirmed PKiKP waves at ILAR

Date	Time	Lat. (°N)	Lon. (°E)	Dep. (km)	Dis. (°)	mb	Ratios†	
							PREM	This Study
1996/10/19	14:53:48	−20.41	−178.51	591.0	88.46	6.1	45.8	2.0
1996/11/14	13:47:38	−21.24	−176.62	192.0	88.88	5.9	52.6	2.5
1997/03/11	03:13:59	−21.13	−178.86	553.0	89.23	5.2	63.3	1.4
1997/08/25	11:59:00	−20.80	−177.78	394.0	88.69	5.3	36.1	1.7
1998/10/26	02:34:57	−21.22	−178.90	573.9	89.33	4.9	94.0	1.5
1999/02/10	09:22:35	−21.71	−178.84	548.9	89.79	5.1	374.7	1.2
1999/06/02	07:34:41	−20.86	−179.00	644.0	89.00	5.0	57.0	1.4
1999/06/26	22:05:28	−17.96	−178.19	590.4	86.01	5.3	11.0	1.2
1999/07/21	03:10:44	−18.29	−177.91	560.8	86.27	5.4	16.5	1.8
1999/11/30	20:10:22	−21.33	−178.66	547.9	89.39	5.3	93.2	1.5
1998/09/16	02:12:02	−6.58	154.87	87.0	83.10	5.4	10.7	1.8
1998/07/16	11:56:36	−11.04	166.16	110.2	83.46	6.4	2.7	0.5
1999/02/05	11:39:45	−12.62	166.97	213.0	84.71	5.7	0.7	0.1
1999/08/02	09:47:12	−12.55	167.18	251.2	84.58	5.3	1.2	0.2

† These ratios are determined as $\frac{PKiKP_{obs}/P_{obs}}{PKiKP_{theo}/P_{theo}}$, where the theoretical values are computed using PREM ($\Delta P_{ICB}=0.67$ km/s, $\Delta S_{ICB}=3.5$ km/s, and $\Delta\rho_{ICB}=0.60$ g/cm^3) and the model determined in this study ($\Delta P_{ICB}=0.67$ km/s, $\Delta S_{ICB}=2.82$ km/s, and $\Delta\rho_{ICB}=0.52$ g/cm^3).

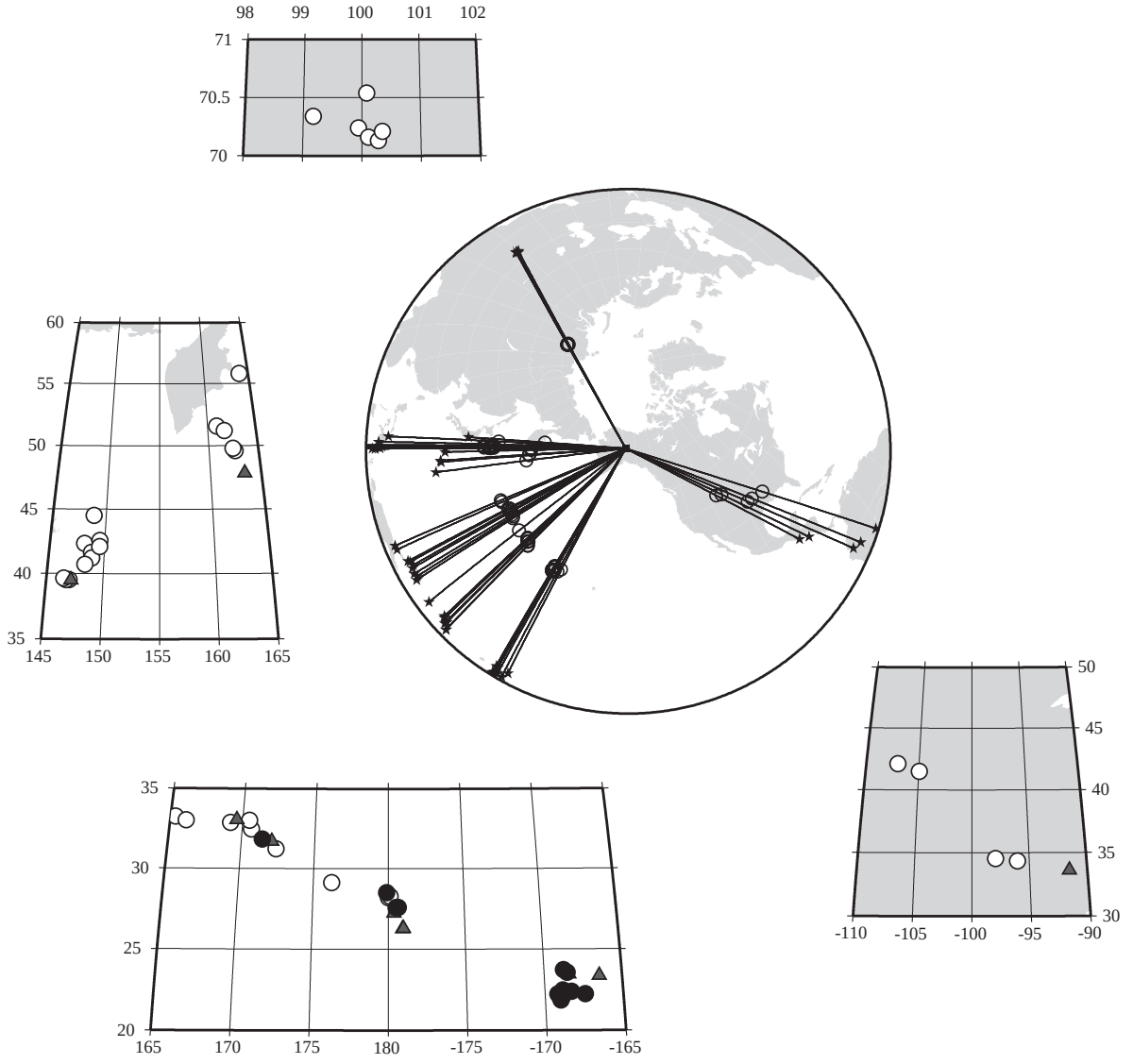

Fig. 6. The center panel shows an ILAR-centered projection of all the events recorded at ILAR and analyzed in this study. The stars indicate epicenters and the circles indicate ICB bounce points. The four surrounding panels show close-ups of the ICB bounce points, with positive observations represented by black circles, inconclusive observations represented by grey triangles, and negative observations represented by white circles.

Fig. 6, and the optimal array beams for these events are presented in Fig. 7.

4. Robustness of the PKiKP observations

Because many of the ILAR data appear to have such anomalously big PKiKP waves we carried out several tests on the robustness of the positive observations before considering the implications for ICB structure. First we doublechecked the identity of the PKiKP waves by making accurate estimates of the arrival time. We handpicked PKiKP and P arrival times from optimal array beams and found that the resulting differential PKiKP–P travel times had a mean of 1.41 s and a standard deviation of 0.82 s

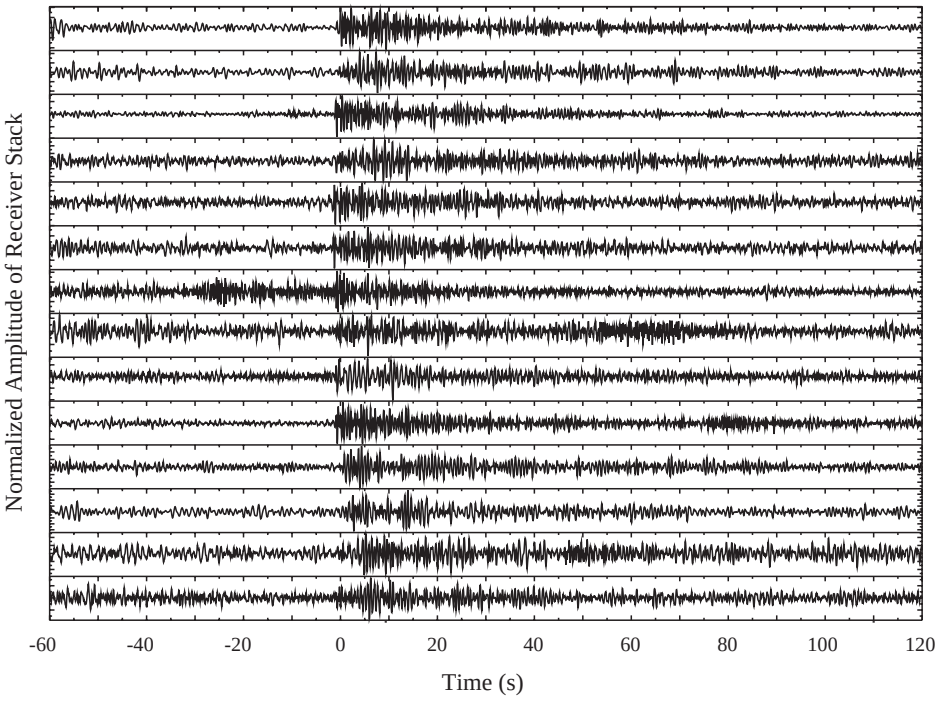

Fig. 7. Linear receiver beams for the 14 events at ILAR that were positive for the presence of PKiKP. Each beam was formed using the theoretical PKiKP slowness vector and a 3-pole Butterworth bandpass filter centered at 4 Hz and two octaves wide. The zero time is the theoretical PKiKP travel time to the beam reference point. Source information for these events is listed in Table 1.

with respect to PREM. The observational uncertainty in making the picks was about 0.25 s, therefore the positive mean of the residuals is probably significant in terms of Earth structure. It implies that either the P waves are fast, which is unlikely since they traverse the large, slow superplume structure in the Pacific, or that the PKiKP waves are slow. However, the travel time residual is not large enough to imply that PKiKP is being misidentified.

We next attempted to improve the accuracy of our method for inferring 2D slowness vectors. The small apertures of ILAR and other IMS arrays often lead to slowness anomalies of 1–2 s/deg if corrections for intra-array variations in topography and geology are not used. These can be implemented either by using explicit slowness–backazimuth station corrections after a standard inference of the 2D slowness vector is made (e.g., [22]), or by applying static corrections to traces before the 2D slowness vector is inferred (e.g., [23]). We chose the latter method and incorporated the recent ILAR statics of Lindquist et al. [24] into our grid search technique. The resulting ray parameter residuals for the positive PKiKP observations at ILAR had a mean of -0.26 s/deg and a standard deviation of 0.36 s/deg, and so were not anomalous. The backazimuth residuals were more significant, with a mean of 52.4° clockwise and a standard deviation of 25.4°. These angular residuals are not as extreme as they might appear because the ray parameters are so low, however they do imply that the PKiKP ray paths have been bent anomalously to the northwest. Interestingly, the P waves lack any slowness anomalies, with ray parameter residuals of -0.12 ± 0.44 s/deg and backazimuth residuals of only $5.7 \pm 3.4°$ clockwise. In sum, the travel time, ray parameter, and backazimuth estimates all suggest that PKiKP is being properly identified.

We also considered the possibility that the large PKiKP/P amplitude ratios recorded at ILAR were being created by unusually small P waves, rather than unusually large PKiKP waves. We examined the Reviewed Event Bulletin of the prototype International Data Center, which often reports single-station estimates for mb as well as the average mb for the

IMS network. For the anomalous Tonga–Fiji events the mb value based on the ILAR P wave was an average of 0.25 units higher than the network averaged mb value. In other words, the P waves recorded at ILAR are themselves anomalously large, and act to reduce the PKiKP/P amplitude ratios.

Next we considered the robustness of our technique for measuring the PKiKP/P amplitude ratios. Small changes to the parameters of the bandpass filter (a 2-pole Butterworth filter with corners at 1.0 and 3.0 Hz) had little effect. However, there was a significant increase in PKiKP/P amplitude ratios at higher frequencies, with an increase of about 30% for a filter centered at 4 Hz. We then tried measuring the ratios from array beams created by aligning all the traces without requiring that the differential times fit a plane wave model. This led to systematically larger estimates for individual phases because some of the destructive interference created by site effects was eliminated. However, there was no systematic effect on the amplitude ratios, and the PKiKP/P observations changed by an average of only 5%.

It is important to point out that the predicted PKiKP/P ratios were calculated using the ray theoretical expression for the reflection coefficient at the ICB, and that this expression becomes inaccurate as distances approach the point of critical reflection (~110°). However, previous studies have shown that the effect of finite frequencies at precritical distances is to reduce the reflection coefficient from its ray theory value, and to shift the point of maximum amplitude to larger distances [25,26]. Thus the true model predictions for PKiKP/P amplitude ratios are probably slightly lower than what is shown in Fig. 5, at least at the large distances, making the observed PKiKP/P amplitudes that much more anomalous with respect to PREM.

A crustal or mantle origin for the anomalously large PKiKP waves recorded at ILAR is unlikely. For instance, although it's possible that a scatterer near the CMB could alter the PKiKP ray path such that it hits the ICB with a larger than expected ray parameter (giving a larger reflection coefficient), the required ray path deviation would lead to an unreasonably large time delay. As a numerical example, if we imagine a PKiKP recorded at 90° that has been scattered at the CMB such that it interacted with the ICB with a ray parameter appropriate for a distance of 110°, we find that it should arrive about 32 s after the expected time. The same argument would hold for any ray path bending associated with velocity heterogeneities: any structure anomalous enough to significantly alter the incidence angle at the ICB would lead to an enormous travel time anomaly.

The most credible method for generating anomalously large PKiKP waves without appealing to nonstandard structure at the ICB is by some sort of geometrical focusing in the mantle. Distortion of the PKiKP waveforms by the Aleutian slab is possible, especially since the anomalous waves arrive at ILAR along the strike direction of the subduction zone; however, the PKiKP ray paths are nearly vertical and the Aleutian slab has a shallow dip [27] so the distortion is likely to be small. Furthermore, it's unclear why the slab would distort PKiKP and P differently, because the ray paths are similar at shallow depths. A more likely region for anomalous focusing is the lowermost mantle. This region is well-known for being laterally heterogeneous, and the PKiKP waves sample it much differently than the corresponding P waves (Fig. 1). It is also known that there are strongly anomalous ultra-low-velocity-zones near the source-side CMB pierce points of the ILAR data [28]. However, it is difficult to imagine how such a structure could cause an amplification of one to two orders of magnitude in the PKiKP amplitude. Although focusing effects may be more prominent for the high frequencies considered here, a recent global study of P wave focusing for periods near 5 s found amplitude variations of only 30–40% [29].

5. Models of the ICB

Before jointly modeling the PKiKP/(P, PcP) amplitude ratios we revised the original PKiKP/PcP amplitude ratios ([10], hereafter referred to as KP04). In that study the authors did not account for the effect of the source in influencing PKiKP/PcP amplitude ratios. Although at small distances PcP and PKiKP leave at very similar take-off angles, and so should be similarly excited by the source, some variation is possible. Harvard CMT solutions [21] were available for 237 of the 279 observations in KP04, and using these solutions we calculated ratios between PKiKP and PcP radiation pattern coefficients (Fig. 8). The mean is

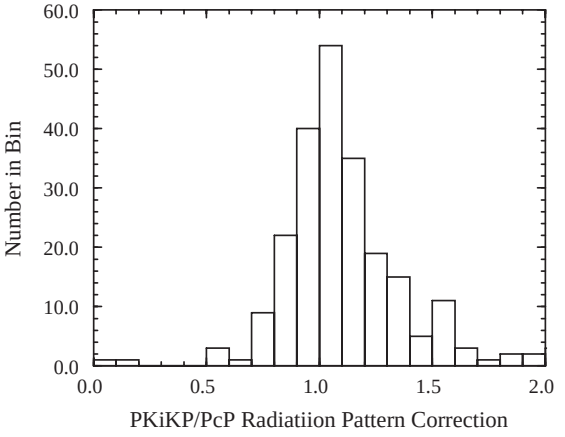

Fig. 8. Distribution of radiation pattern corrections for the PKiKP/PcP amplitude ratio data base developed in a previous study [10]. The effect of these corrections is minor because the mean is near one, the distribution is symmetric, and about 80% of the values fall between 0.75 and 1.25.

near one, the distribution is symmetric, and about 80% of the corrections fall within 0.75 and 1.25. Therefore, application of the corrections is unlikely to dramatically affect the inferred values of $\Delta\rho_{ICB}$ and ΔS_{ICB}. Nevertheless, in this study we proceed using the revised PKiKP/PcP data set.

Both the scatter in positive PKiKP/P amplitude ratios and the variability in observing PKiKP are large (Fig. 5), and probably indicate some level of complexity at the ICB. Although the data tend to be coherent geographically, there is no completely self-consistent manner in which to combine the positive observations with the negative observations to infer a global average for ICB properties. As a compromise, we defined a proxy PKiKP/P curve to use in our modeling. The curve is defined as

$$\mathrm{PKiKP/P} = 0.001133 \times \Delta - 0.07700,$$
$$75.0^\circ \le \Delta \le 90.0^\circ \quad (1)$$

and is presented in Fig. 9. The proxy curve was chosen to honor as many of the binned negative observations as possible, while not straying too far away from the binned positive observations. The inconclusive data were disregarded in this approach. We defined the proxy curve only for the distance range in which there were significant numbers of both positive and negative observations, although the slope of the curve was chosen such that models which match it will tend to honor the negative observations in the distance range of 50–75°.

We first considered models of the ICB which are constrained only by the PKiKP/P proxy curve. We fixed ΔP_{ICB} to the value given by PREM, and systematically varied ΔS_{ICB} and $\Delta\rho_{ICB}$ in a grid search. The misfit was calculated using an L2 norm and the results are presented in Fig. 9. The proxy curve is effective at constraining ΔS_{ICB} but has little effect on $\Delta\rho_{ICB}$, as is expected from the sensitivity curves shown in Fig. 2. The objective function has two valleys of local minima because we considered only the absolute value of PKiKP/P amplitude ratios. One valley corresponds to positive ratios and the other corresponds to negative ratios of roughly equal magnitude. We experimented with different sampling densities of the proxy-curve and found this has little effect on the results.

Next we present the results of a similar grid search using only the revised PKiKP/PcP data set. In this case ΔP_{ICB} was again held fixed, and a weighted L2 norm was used to calculate the misfit. There is a single broad valley in this case, indicating significant uncertainty in both parameters, however a distinct minimum exists at $\Delta S_{ICB}=2.025$ km/s and $\Delta\rho_{ICB}=0.400$ g/cm^3. The differences with respect to the values previously reported in KP04 ($\Delta S_{ICB}=2.0$ km/s and $\Delta\rho_{ICB}=0.3$ g/cm^3) are owing to the finer grid search used in the current study, the effect of the source mechanism corrections, and the elimination of the PKiKP/PcP data that were associated with earthquakes too small to have CMT solutions. We estimated errors for the parameters using a bootstrap type process in which multiple realizations of the data set were created by sampling Gaussian pdfs. The pdfs were constructed using the observed data values as means and the estimated uncertainties as standard deviations. A grid search was conducted on each realization of the data set and the population of optimal solutions was used to estimate the model covariance matrix. The corresponding 95% confidence ellipse is shown centered on the original optimal solution (Fig. 9).

In the third grid search we combined the PKiKP/P and PKiKP/PcP data sets. A weighted L2 norm was used and each PKiKP/P point along the proxy line was assigned an observational error equivalent to the mean of the errors of the PKiKP/PcP data. This led to equal treatment of both data sets. A distinct minimum

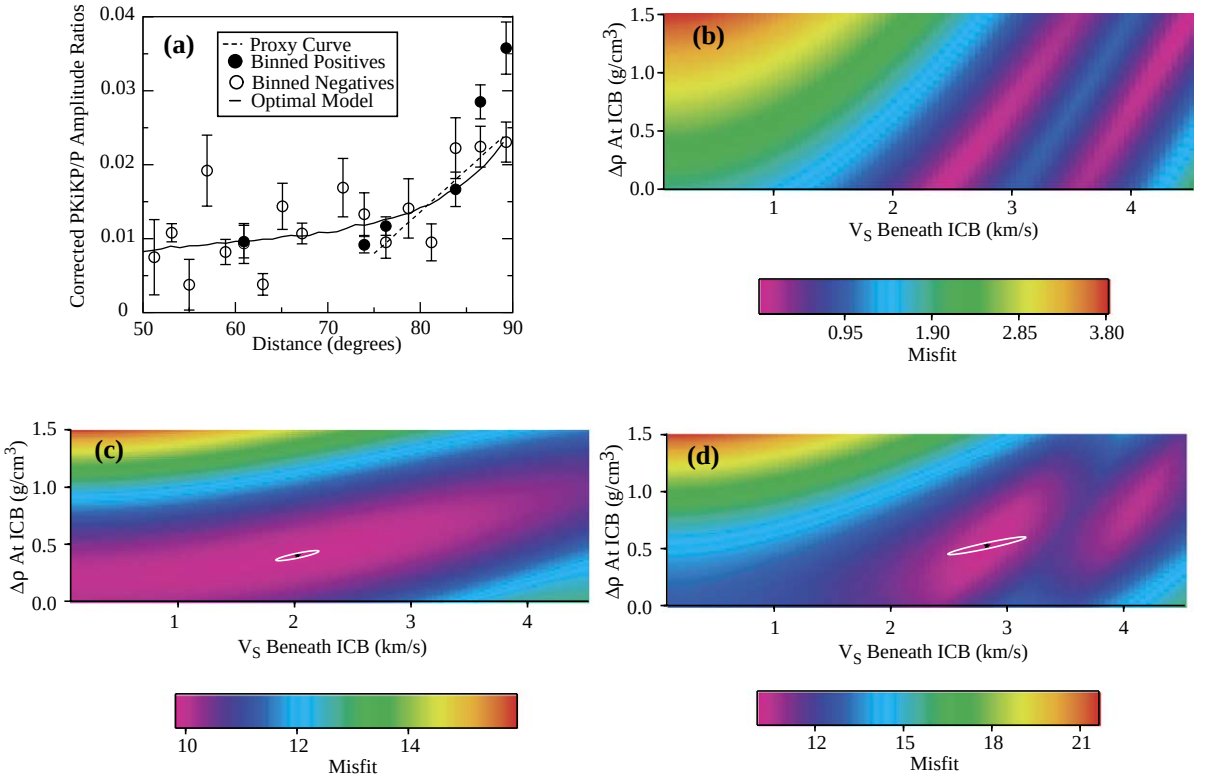

Fig. 9. (a) The averaged positive and negative PKiKP/P observations as shown in Fig. 5. The dashed line indicates the relationship used as a proxy for the observed PKiKP/P amplitude ratio, and the solid line shows the predictions for the optimal model found in this study. (b) The objective function for the PKiKP/P proxy line. (c) The objective function for the revised PKiKP/PcP data. (d) The objective function for the combination of the two data sets. The ellipses represent 95% confidence areas determined from a bootstrap technique and reflect only the uncertainty related to observing the data; they do not account for the larger bias caused by uncertainties in the assumed model of the CMB and ΔP_{ICB}.

occurs at $\Delta S_{ICB}=2.825$ km/s and $\Delta\rho_{ICB}=0.525$ g/cm^3. The predicted PKiKP/P amplitude ratios for this model are shown in Fig. 9.

It is critical to point out that the error ellipses (Fig. 9) are based only on estimates of observational uncertainties and do not account for underlying assumptions in the modeling. The most important of these is the assumption that ΔP_{ICB} and all of the properties of the core–mantle boundary (CMB) are exactly matched by PREM. In an attempt to quantify this bias we used a model resampling technique that is analogous to the data resampling technique. We generated Gaussian pdfs for ΔP_{ICB} and all of the CMB properties using PREM values for the means of the pdfs. The standard deviations were assigned as 2.5% of the mean for the P and S velocity above the CMB, and 1% of the mean for the remaining parameters. We then selected a model

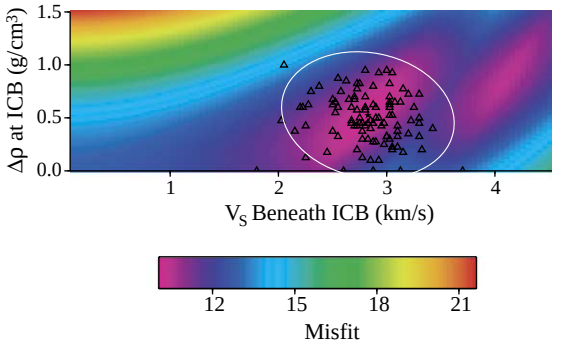

Fig. 10. Results of the model resampling process used to estimate uncertainties in ΔS_{ICB} and $\Delta\rho_{ICB}$ caused by assuming PREM values for ΔP_{ICB} and the structure above and below the CMB. The 95% confidence ellipse is shown in white, and is defined by the covariance matrix calculated from 100 bootstrap solutions, shown by triangles.

and performed the grid search to find the optimal values of ΔS_{ICB} and $\Delta\rho_{ICB}$. This process was repeated and the population of solutions was used to estimate uncertainties for the two relevant model parameters. Combining this procedure with the data resampling process we found a much larger 95% confidence ellipse (Fig. 10), and 1σ uncertainties of $\Delta S_{ICB}=2.825\pm0.326$ km/s and $\Delta\rho_{ICB}=0.525\pm0.240$ g/cm^3.

6. The density jump across the ICB

Considering all the caveats in our modeling and the quantitative estimates of the uncertainties, the difference between the value for $\Delta\rho_{ICB}$ reported here (0.525 g/cm^3) and the standard PREM value (0.6 g/cm^3) is not significant. However, the current value does appear significantly different than the results of a recent study of PKiKP/PcP amplitudes [11]. In that study (hereafter referred to as CR04) the authors found that $\Delta\rho_{ICB}=0.85$ g/cm^3 when ΔP_{ICB} was fixed at the PREM value. Although there are subtle differences in the modeling approaches of CR04 and this study, the large difference in inferred $\Delta\rho_{ICB}$ values is mainly owing to differences in the PKiKP/PcP data sets. The values used by CR04 were systematically higher than those used here, and so it follows that CR04 found a substantially higher value for $\Delta\rho_{ICB}$.

One possibility why the current data set has on average lower PKiKP/PcP ratios than the CR04 data set is that the former was developed using small-aperture array stations and the latter was developed mainly from individual broadband seismometers. The array stations permit a lower threshold of detection for PKiKP waves and so have the capability of observing smaller PKiKP/PcP ratios. A second point is that many individual PKiKP/PcP data in the current study are comparable in magnitude to the CR04 data, and it is only the averaged values which are systematically smaller than the CR04 data. The larger number of observations used here as compared to CR04 may lead to a more robust average because of the inherent scatter in high-frequency body wave amplitudes. It is also relevant that many of the small PKiKP/PcP ratios used in the current study have small uncertainties and so play a large role when the data are binned or fit with a weighted norm. It is debatable whether this is an unwelcome bias, however it does explain some of the discrepancy between the data sets. It has also been suggested that the array based PKiKP/PcP amplitude ratios may be systematically degraded by destructive inference in the array beams caused by intra-array site effects. While we do find that individual phase amplitudes are degraded by such a phenomenon, there is no systematic effect on the amplitude ratios. For instance, the PKiKP/P amplitude ratios changed by an average of 5% when we accounted for this effect, and the changes were not consistently positive or negative.

The current estimate of $\Delta\rho_{ICB}=0.525\pm0.239$ g/cm^3 also appears somewhat different than the recent mode derived value of $\Delta\rho_{ICB}=0.82\pm0.18$ g/cm^3 [9]. In this case a reasonable Earth structure explanation is plausible because of the different sensitivities of the two types of data. The mode data have broad, depth dependent sensitivity kernels; for instance, the radial resolving length of the relevant mode data set is approximately 140 km for a 10% level of uncertainty at the ICB depth [9]. The body wave data, although biased by crustal and mantle structure, technically offer density constraints within at most half a wavelength (<5 km) of the ICB. Therefore it is possible that the existence of a relatively thin layer, with density intermediate between the outer core and the bulk of the inner core, could satisfy both types of estimates.

The discrepancy between the mode-based and PKiKP-based estimates for $\Delta\rho_{ICB}$ may also be resolvable by changing one of the assumptions commonly used in modeling modes (written communication, M. Rochester, 2004). While most mode-based reference Earth models are constrained using an inertia coefficient of 0.3308 it may be more appropriate to use a value of 0.332, because the latter value is more consistent with the observed flattening of the Earth [31]. Although the difference appears subtle, it has been suggested that the increase in the inertia coefficient leads to a reduction of $\Delta\rho_{ICB}$ from the standard PREM value of 0.6 to 0.37 g/cm^3 [4]. Such an argument may also apply to the more recent mode-based value as well.

7. The shear velocity at the top of the inner core

Although there is disagreement among the PKiKP-based studies on $\Delta\rho_{ICB}$, there seems to be a consensus

that ΔS_{ICB} is significantly smaller than the mode-based PREM value of 3.5 km/s. This is suggested not just by the recent PKiKP studies but also by older studies based on waveform modeling [30,32,33]. The apparent discrepancy may be related to the different frequency bands of the seismic observations: inner core sensitive modes are observed at frequencies in the milliHertz range, while PKiKP waves are observed at frequencies about three orders of magnitude higher. Physical dispersion, which would lead to higher frequencies sensing a higher velocity (opposite of the observations) probably plays a small role. Assuming a simple viscoelastic model and using a conservative estimate of 0.01 for the maximum of a frequency dependent Q^{-1}, the maximum percentage change in phase velocity is only about 1% [34]. It's more likely that the apparent discrepancy can be reconciled in the same manner as the competing $\Delta\rho_{ICB}$ estimates, essentially by geometrical dispersion. PKiKP based studies constrain only the outermost few kilometers of the inner core, while the radial resolving length for shear velocity below the ICB has been estimated to be about 175 km for a 10% level of uncertainty [9]. Therefore, a thin layer of anomalously reduced shear velocity at the top of the inner core can explain both the mode and body-wave data simultaneously. But because the inner core is nearly isothermal and the pressure dependence of the shear velocity of hcp-iron is small at inner core conditions [35], there should be little depth dependence to the shear velocity profile in the inner core. Therefore in order to reconcile the current value of 2.8 km/s for ΔS_{ICB} with the well-constrained value of 3.6 km/s for the mean S-velocity in the inner core [5] the anomalous layer at the top of the inner core must be different in chemistry (perhaps more light element) or structure (perhaps more partial melt) from the bulk of the inner core.

8. Lateral heterogeneity at the ICB

The PKiKP/P amplitude ratios presented in Fig. 5 show a dramatic amount of variability. In many cases, a negative observation yields an upper-limit estimate of the PKiKP/P amplitude ratio that is much lower than a PKiKP/P amplitude ratio measured directly from a positive observation. And even among the positive observations, estimated PKiKP/P amplitudes vary by almost two orders of magnitude. However, it is important to note that there is significant geographical coherence to this variation. For example, at ILAR 13 of the 14 anomalously large PKiKP/P amplitude ratios came from events that occurred in the Tonga–Fiji subduction zone. An additional three events from the New Hebrides trench yielded positive PKiKP observations at ILAR, but showed significantly lower PKiKP/P amplitude ratios. Furthermore, the cluster of four positive PKiKP observations near 74° all came from events that occurred in the New Hebrides trench and were recorded at the Chiang Mai array (CMAR) in Thailand.

Undoubtedly, factors such as focusing caused by 3D variations in the mantle account for some of the geographical variation in PKiKP/P amplitude ratios, but it is unlikely that all of the variation can be accounted for in this manner. It is more likely that a component of this apparent scatter is created by lateral heterogeneity at the ICB itself. One possibility for the complexity is small wavelength topography on the ICB. Depending on the ray parameter a slope of 5–10° can provide significant variations in PKiKP amplitude, although it's unlikely that such a steep slope could be sustained in the low-viscosity inner core. A second possibility is the presence of scatterers lying at the base of the outer core. Such features would presumably have density intermediate between the inner and outer cores, and reflect part of the sedimentation and compaction process that grows the inner core. As a third possibility, it may be that the ICB is itself homogeneous but that a few kilometers below are strong scatterers. This could help explain the slight time delay and azimuthal anomaly of the PKiKP arrivals recorded at ILAR. Strong heterogeneities within the outer inner core have been hypothesized to exist based on observations of PKiKP coda waves [16], and the data presented here do possess long coherent codas of low slowness energy [20].

9. Conclusions

Modeling of a combined data set of PKiKP/PcP and PKiKP/P amplitude ratios leads to values of $\Delta S_{ICB} = 2.82 \pm 0.32$ km/s and $\Delta\rho_{ICB} = 0.52 \pm 0.24$ g/

cm^3. Because of the large scatter in the data, and the assumptions necessary in the modeling process, the difference between this estimate of $\Delta\rho_{ICB}$ and the standard PREM value of 0.60 g/cm^3 is not significant. Compared to the recent mode-based estimate of 0.82 ± 0.18 g/cm^3 [9] the value reported here is different at only a modest level of significance. This difference may be due to modeling assumptions but could also indicate an Earth structure effect in which a relatively thin, anomalous layer exists at the top of the inner core. Such a layer would also help explain the more significant difference between the value of ΔS_{ICB} reported here, and the standard PREM value of 3.5 km/s.

Currently, it is thought that a mushy, partially molten layer near the ICB (e.g., [36]) would be negligibly thin (about 10 m) because the viscous compaction of the solid iron matrix would be extremely efficient at expelling fluid [37]. This thickness estimate relies on a value of 10^{16} Pa s for the viscosity of solid iron at core conditions and if the newer estimate of 10^{11} Pa s [38] is used the hypothetical mushy layer becomes even thinner. However, distinct from the idea of a thin, mushy, high melt-fraction layer at the top of the inner core is the idea of a thicker (~200 km) "crust-like" layer of abnormally low partial melt content in the outermost inner core [39]. Interestingly, there is seismic evidence for a change in material properties near this depth, with some researchers suggesting a gradual transition from isotropy to anisotropy at a depth of 200–300 km below the ICB [40,41]; it's unclear whether such a layer would have a significantly lower density and shear velocity than the bulk of the inner core, but if so it could help reconcile the competing seismic estimates of ICB properties.

The large variation, but geographical coherence, of our PKiKP/P ratios suggest that significant heterogeneity exists at, or very near, the ICB. This idea is supported by recent waveform modeling of PKP phases that identifies a low velocity zone at the top of the inner core beneath India [42], and by anomalous observations of precritical PKiKP amplitudes from nuclear weapons tests in the former Soviet Union [43]. It has also been suggested that the high-frequency coda waves observed to follow precritical PKiKP are created not from volumetric heterogeneities within the inner core but from a complicated, multi-layered ICB structure [44]. The seismic evidence is thus becoming more compelling that the process responsible for growing the inner core is not uniformly simple.

Acknowledgments

This work was supported by National Science Foundation under grants EAR-0229103 and EAR-0296078. We thank the prototype International Data Center for the IMS array data, and the Harvard CMT Project for moment tensors. Most of the figures were created using GMT [45]. We thank S. Rost and an anonymous referee for constructive reviews.

References

[1] F.D. Stacey, C.H.B. Stacey, Gravitational energy of core evolution: implications for thermal history and geodynamo power, Phys. Earth Planet. Inter. 110 (1999) 83–93.
[2] J. Hinderer, D.J. Crossley, O.G. Jensen, A search for the Slichter triplet in superconducting gravimeter data, Phys. Earth Planet. Inter. 90 (1995) 183–195.
[3] J. Hinderer, D.J. Crossley, Core dynamics and surface gravity changes, Dynamics of Earth's Deep Interior and Earth Rotation, AGU Geophys. Mono. 72, vol. 12, 1993, pp. 1–16.
[4] C. Denis, Y. Rogister, M. Amalvict, C. Delire, A. Ibrahim Denis, G. Munhoven, Hydrostatic flattening, core structure, and translational mode of the inner core, Phys. Earth Planet. Inter. 99 (1997) 195–205.
[5] A.M. Dziewonski, D.L. Anderson, Preliminary reference Earth model, Phys. Earth Planet. Inter. 25 (1981) 297–356.
[6] T.G. Masters, P.M. Shearer, Summary of seismological constraints on the structure of the Earth's core, J. Geophys. Res. 95 (1990) 21691–21695.
[7] A. Souriau, M. Souriau, Ellipticity and density at the inner core boundary from subcritical PKiKP and PcP data, Geophys. J. Int. 98 (1989) 39–54.
[8] P. Shearer, G. Masters, The density and shear velocity contrast at the inner core boundary, Geophys. J. Int. 102 (1990) 491–498.
[9] G. Masters, D. Gubbins, On the resolution of density within the Earth, Phys. Earth Planet. Inter. 140 (2003) 159–167.
[10] K.D. Koper, M.L. Pyle, Observations of PKiKP/PcP amplitude ratios and implications for Earth structure at the boundaries of the liquid core, J. Geophys. Res. 109 (2004) B03301, doi:10.1029/2003JB002750.
[11] A. Cao, B. Romanowicz, Constraints on density and shear velocity contrasts at the inner core boundary, Geophys. J. Int. 157 (2004) 1146–1151.
[12] M. Ishii, A.M. Dziewonski, J. Tromp, G. Ekström, Joint inversion of normal mode and body wave data for inner core

anisotropy 2. Possible complexities, J. Geophys. Res. 107 (2002) 2380, doi:10.1029/2001JB000713.
[13] J. Tromp, Inner-core anisotropy and rotation, Annu. Rev. Earth Planet. Sci. 29 (2001) 47–69.
[14] S. Tanaka, H. Hamaguchi, Degree one heterogeneity and hemispherical variation of anisotropy in the inner core from PKP(BC)-PKP(DF) times, J. Geophys. Res. 102 (1997) 2925–2938.
[15] K. Creager, Large-scale variations in inner core anisotropy, J. Geophys. Res. 104 (1999) 23127–23139.
[16] J.E. Vidale, P.S. Earle, Fine-scale heterogeneity in the Earth's inner core, Nature 404 (2000) 273–275.
[17] F.L. Niu, L.X. Wen, Hemispherical variations in seismic velocity at the top of the Earth's inner core, Nature 410 (2001) 1081–1084.
[18] L. Wen, F. Niu, Seismic velocity and attenuation structures in the top of the Earth's inner core, J. Geophys. Res. 107 (2002) 2273, doi:10.1029/2001JB000170.
[19] X. Song, Three-dimensional structure and differential rotation of the inner core, Earth's Core; Dynamics, Structure, Rotation, Geodynamics Series, vol. 31, 2003, pp. 45–63.
[20] K.D. Koper, J.M. Franks, M. Dombrovskaya, Evidence for small-scale heterogeneity in Earth's inner core from a global study of PKiKP coda waves, Earth Planet. Sci. Lett. 228 (2004) 227–241.
[21] See www.seismology.harvard.edu/projects/CMT.
[22] I. Bondar, R.G. North, G. Beall, Teleseismic slowness–azimuth corrections for the International Monitoring System seismic network, Bull. Seismol. Soc. Am. 89 (1999) 989–1003.
[23] I. Tibuleac, G. Herrin, Calibration studies at TXAR, Seismol. Res. Lett. 68 (1997) 353–365.
[24] K.G. Lindquist, I.M. Tibuleac, R.A. Hansen, A semi-automatic calibration method applied to a small-aperture Alaskan seismic array, Bull. Seism. Soc. Am. (2005) submitted for publication.
[25] V. Červený, The amplitude–distance curves for waves reflected at a plane interface for different frequency ranges, Geophys. J. R. Astron. Soc. 13 (1967) 187–196.
[26] V.F. Cormier, P.G. Richards, Full wave theory applied to a discontinuous velocity increase: the inner core boundary, J. Geophys. 43 (1977) 3–31.
[27] O. Gudmundsson, M. Sambridge, A regionalized upper mantle (RUM) seismic model, J. Geophys. Res. 103 (1998) 7121–7136.
[28] M.S. Thorne, E.J. Garnero, Inferences on ultralow-velocity zone structure from a global analysis of SPdKS waves, J. Geophys. Res. 109 (2004) B08301, doi:10.1029/2004JB003010.
[29] I.M. Tibuleac, G. Nolet, C. Michaelson, I. Koulakov, P wave amplitudes in a 3-D earth, Geophys. J. Int. 155 (2003) 1–10.
[30] G.L. Choy, V.F. Cormier, The structure of the inner core inferred from short-period and broadband GDSN data, Geophys. J. R. Astron. Soc. 72 (1983) 1–21.
[31] C. Denis, M. Amalvict, Y. Rogister, S. Tomecka-Suchon, Methods for computing internal flattening, with applications to the Earth's surface and geodynamics, Geophys. J. Int. 132 (1998) 603–642.
[32] H. Häge, Velocity constraints for the inner core inferred from long period PKP amplitudes, Phys. Earth Planet. Inter. 31 (1983) 171–185.
[33] P. Cummins, L.R. Johnson, Short-period body wave constraints on properties of the Earth's inner core boundary, J. Geophys. Res. 93 (1988) 9058–9074.
[34] S. Stein, M. Wysession, An Introduction to Seismology, Earthquakes, and Earth Structure, Blackwell Publishing, 2003, p. 197.
[35] D. Antonangeli, F. Occelli, H. Requardt, J. Badro, G. Fiquet, M. Krisch, Elastic anisotropy in textured hcp-iron to 112 GPa from sound wave propagation measurements, Earth Planet. Sci. Lett. 225 (2004) 243–251.
[36] D.R. Fearn, D.E. Loper, P.E. Roberts, Structure of the Earth's inner core, Nature 292 (1981) 232–233.
[37] I. Sumita, S. Yoshida, M. Kumazawa, Y. Hamano, A model for sedimentary compaction of a viscous medium and its application to inner-core growth, Geophys. J. Int. 124 (1996) 502–524.
[38] James A. Van Orman, On the viscosity and creep mechanism of Earth's inner core, Geophys. Res. Lett. 31 (2004) L20206, doi:10.1029/2004GL021209.
[39] I. Sumita, S. Yoshida, Thermal interactions between the mantle, outer and inner cores, and the resulting structural evolution of the core, in: V. Dehant, K.C. Creager, S. Karato, S. Zatman (Eds.), Earth's Core: Dynamics, Structure, Rotation, AGU Monograph, 2003, pp. 213–231.
[40] X. Song, D.V. Helmberger, Seismic evidence for an inner core transition zone, Science 282 (1998) 924–927.
[41] A. Ouzounis, K.C. Creager, Isotropy overlying anisotropy at the top of the inner core, Geophys. Res. Lett. 23 (2001) 4331–4334.
[42] A. Stroujkova, V. Cormier, Regional variations in the uppermost layer of the Earth's inner core, J. Geophys. Res. 109 (2004) B10307, doi:10.1029/2004JB002976.
[43] D.N. Krasnoshchekov, P.B. Kaazik, V.M. Ovtchinnikov, Seismological evidence for mosaic structure of the surface of the Earth's inner core, Nature 435 (2005) 483–487.
[44] G. Poupinet, B.L.N. Kennett, On the observation of high frequency PKiKP and its coda in Australia, Phys. Earth Planet. Inter. 146 (2004) 497–511.
[45] P. Wessel, W.H.F. Smith, Free software helps map and display data, EOS Trans. Am. Geophys. Union 72 (1991) 441, 445–446.